Doubly resonant distributed feedback cavity with controllable wide wavelength separation

Zhengrui Tu, Jianhao Zhang, Carlos Alonso-Ramos, Xavier Le Roux, Laurent Vivien, Eric Cassan

Optics Communications 494 (2021) 127064

Doubly resonant distributed feedback cavity with controllable wide wavelength separation

Zhengrui Tu *, Jianhao Zhang, Carlos Alonso-Ramos, Xavier Le Roux, Laurent Vivien, Eric Cassan

Université Paris-Saclay, CNRS, Centre de Nanosciences et de Nanotechnologies, 91120, Palaiseau, France

ARTICLE INFO

Keywords:
Silicon nitride
Double resonance waveguide cavity
Bragg mirrors

ABSTRACT

A double corrugation quarterly wavelength shifted (QWS) distributed feedback (DFB) Bragg grating cavity which includes two sets of Bragg gratings located at different positions away from a waveguide center is proposed. It can support two wavelength-far-separated resonances, for instance 735 nm and 1310 nm as an illustrative example of the proposed flexible approach applied to a silicon nitride rib waveguide. Based on the proposed design principle, the two sets of Bragg distributed corrugations operate nearly independently, diffraction losses being minimized by design principle even though these two resonances are widely separated. The proposed approach of a double corrugation cavity that relies on a single-etching fabrication process, fits with the need of situations where two simultaneous widely spaced resonances are required, with potential for applications to on-chip amplification, lasing, second harmonic generation, and nonlinear optical process in hybrid integrated waveguides.

1. Introduction

Cavity resonators frequently play a key role in sensing [1–3], modulation [4], amplification [5], lasing [6,7], or the enhancement of nonlinear optical processes [8–11]. Some key applications also require two or more resonances simultaneously. For example, in the field of nonlinear optical interactions such as parametric amplification or frequency conversion based on degenerate four wave mixing processes, it is desirable to adjust a resonant cavity which can support multiple wavelengths with controllable frequency separation as well as large spatial mode field overlaps. Previous works have addressed this issue and several approaches have been proposed. Micro-ring resonators well support a series of resonances separated by free spectral ranges (FSR) [12], but they can hardly give access to distant resonant frequencies. Photonic crystal (PhC) cavities can provide a strong light confinement with modes having ultra-high quality factors ($Q \gg 10^5$) [13–15] for close target wavelengths [16]. However, in planar PhC structures, higher order bandgaps corresponding to target wavelengths can easily operate above the light line introducing out-of-plane losses. Some works on PhC cavities have addressed the use of bandgaps for different polarizations (TE and TM) to enable two resonant modes in single cavity structures [17]. However, it was found difficult to tune the TE/TM mode frequencies independently as desired, and the fabrication process of structures was made complex by the need of relatively thick membranes to sustain this strategy [18]. In addition, to achieve two arbitrary frequency resonances by circumventing the obstacles mentioned above, crossed nanobeam PhC structures were proposed [18,19] but did not bring a solution to several issues. The quality factor (Q) factor values in such structures were limited to around 10^3 for both resonances due to a limited light confinement ability in the waveguide cross region, meanwhile the spatial overlap between the two resonant modes remained weak. Additionally, these crossed PhC structures also rely on a complicated fabrication process including e-beam lithography, dry etching, as well as wet etching to obtain a nanobeam PhC structure cladded by air. Another work dealing with a doubly resonant cavity structure was reported in [20] where a cavity was formed by placing distributed Bragg reflectors gratings for the pump wavelength on either side of a distributed feedback laser operating at the signal wavelength. Lots of efforts have been devoted to the realization of doubly resonant cavities but the need for a simple design approach of two resonant modes with large frequency separation, acceptable Q factors and nonlinear mode overlaps, compact device size and a flexible control of the resonant mode frequency separation, is still present. In this context, in order to realize two spectrally distant resonant modes in a single on-chip cavity structure, we propose to directly implement a double corrugation distributed feedback cavity at two distinct resonant wavelengths. This approach brings the advantages of simplicity, as shown hereafter, and wavelength on request flexibility.

2. Design principles

We illustrate the proposed methodology by relying on a 600 nm thick silicon nitride (SiN) on SiO_2 wafer case. A partial single-etching

* Corresponding author.
E-mail address: zhengrui.tu@universite-paris-saclay.fr (Z. Tu).

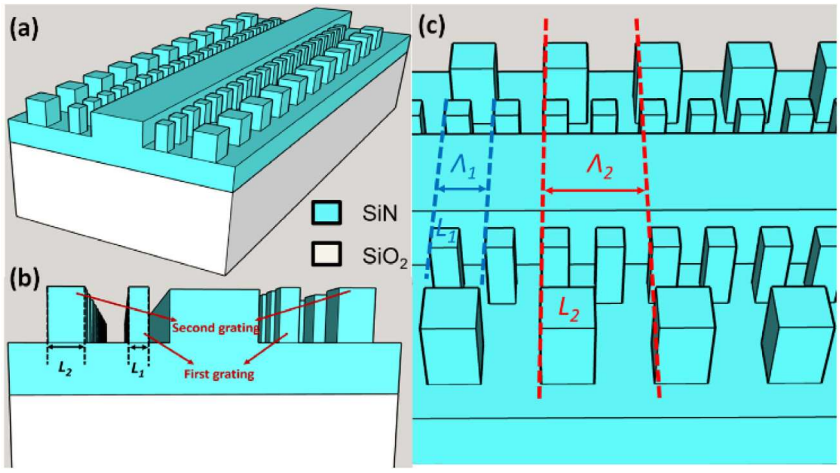

Fig. 1. (a) 3D schematic diagram of the considered double corrugation distributed feedback optical cavity. (b) Cross-section view of the structure: a rib waveguide based on a 600 nm thick SiN (on SiO_2) layer is combined with two series of Bragg gratings. (c) Top view of the structure giving details of the double Bragg gratings.

step is considered to define all gratings, including two couples of Bragg mirrors forming each a quarter-wave shift cavity. Sketches of the proposed double corrugation rib waveguide structure are shown in Fig. 1(a)–(c). The smaller size gratings (inner gratings) close to the rib are designed for the shorter wavelength (~735 nm, λ_1), while the larger size gratings (outer gratings) located farther from the rib are designed for the longer wavelength (~1310 nm, λ_2). They correspond, for example to the pump and signal wavelengths of semiconducting single-wall carbon nanotubes with chirality (8,7) [21], respectively. In such an approach, the key point to be satisfied is the near-independence of each Bragg distributed feedback mechanism with respect to the other one. It is thus a question of defining the conditions that each light spectral window (e.g. around λ_1 and λ_2, respectively) is sensitive to only one of the gratings. The proposed approach consists in ensuring a sufficient distance between the outer gratings and the mode spatial area at the short wavelength, meanwhile operating the inner ones in a sub-wavelength regime [22,23] for the long wavelength spectral window. Note that the sub-wavelength regime here refers to a situation: $\lambda \gg \Lambda$, where λ is the target wavelength and Λ is the grating period.

As a first step, single-mode condition is chosen at both operating wavelengths in TE-like polarization in the considered SiN rib waveguide structure. Typical dimensions are selected based on eigenmode calculation with fabrication feasibility constraints taken into account, as indicated in Fig. 2(a). The SiN core thickness is H_{core} = 600 nm; the width and height of the rib waveguide are W_{rib} = 450 nm, H_{rib} = 350 nm, respectively. The properties of propagative modes at these two wavelengths were estimated with *COMSOL Multiphysics* [24]. The effective index values and the mode profiles of the corresponding modes at the two prescribed wavelengths are given in Figs. 2(c) and 2(d). Their different lateral spreading can be qualitatively observed. The overlap between the modes at the two wavelengths was estimated as 0.818 [25].

Our strategy was to offset the second Bragg gratings from the rib waveguide for significantly reducing the influence on light propagation at and around λ_1. This configuration benefits from the considerable difference between the mode areas at λ_1 and λ_2, estimating them through Eq. (1):

$$A = \frac{(\int |E(x,y)|^2 \, dxdy)^2}{\int |E(x,y)|^4 \, dxdy} \tag{1}$$

where *E(x,y)* is the electrical field intensity and x, y are the dimensions along the waveguide cross-section. A_1 = 0.3668 μm^2 (at λ_1) and A_2 = 0.9136 μm^2 (at λ_2) were obtained accordingly, bringing a confirmation of the appropriate choice of the structure cross-section to ensure a huge difference between the mode areas at the two operating wavelengths.

According to the Bragg's law [26], the grating period for the 1st order Bragg wavelength could be derived from Eq. (2), where Λ is the grating period, λ_B is the 1st order Bragg wavelength, and N_{eff} is the effective refractive index at λ_B:

$$\Lambda = \frac{\lambda_B}{2N_{eff}} \tag{2}$$

Then Λ_1 = 196 nm was obtained for the first grating period and Λ_2 = 392 nm for the second grating period. The Bragg grating filling factors (defined as the ratio of the single grating length to the grating period) were both fixed at 0.5, providing the highest grating coupling coefficients [26]. Simultaneously, the chosen Λ_1 value with respect to λ_2 ensured a satisfying margin with respect to the need to hide the first grating by a sub-wavelength behavior relative to long wavelengths.

Next, we quantitatively investigated the condition to hold to minimize the interaction of the mode profile at λ_1 with the outer gratings. As shown in Fig. 2(b), the gaps between the first and second gratings and the rib waveguide were labeled as Gap_1 and Gap_2, respectively. Bringing the inner gratings as close as possible to the rib was in line with the strategy of decoupling the effects of the two gratings for each of the two wavelengths. We kept Gap_1 = 100 nm to ease the fabrication from an experimental point of view. Then, Gap_2 was scanned within the 300–1000 nm range. The effective refractive index of the short wavelength mode was calculated with structures completely taking into account the full cross-section geometry, as shown in Fig. 2(g). From Fig. 2(g), one can see that when $Gap_2 < 650$ nm, the effective refractive index at λ_1 varies with Gap_2, while it reaches a flat regime above this value. This result leads to a quantitative estimation of the limit to the influence of the second gratings on the optical mode at λ_1. Accordingly, the mode profiles at λ_1 in a rib waveguide having the first gratings only (Gap_1 = 100 nm) and in the rib waveguide structure with both gratings (Gap_1 = 100 nm and Gap_2 = 650 nm) are visually identical (see in Figs. 2(e) and 2(f)). Fixing the second gap value accordingly, the coupling coefficients of λ_1 and λ_2 could be derived as κ_1 = ~7400 m^{-1} and κ_2 = ~3200 m^{-1}, respectively, through coupling mode theory [27–29]. All the related parameters of the proposed double corrugation structure are summarized in Table 1.

3. Simulation results and discussion

Based on the parameters listed in Table 1, we constructed a double corrugation distributed feedback cavity, as depicted in Fig. 3. The 3D geometry was simulated with a commercial 3D-FDTD solver [30]. We set the number of grating periods in each side of the cavity as being N_1 = 2000 and N_2 = 1000 for each of the two gratings, resulting in a ~392 μm total length structure. Transmission spectra and electrical

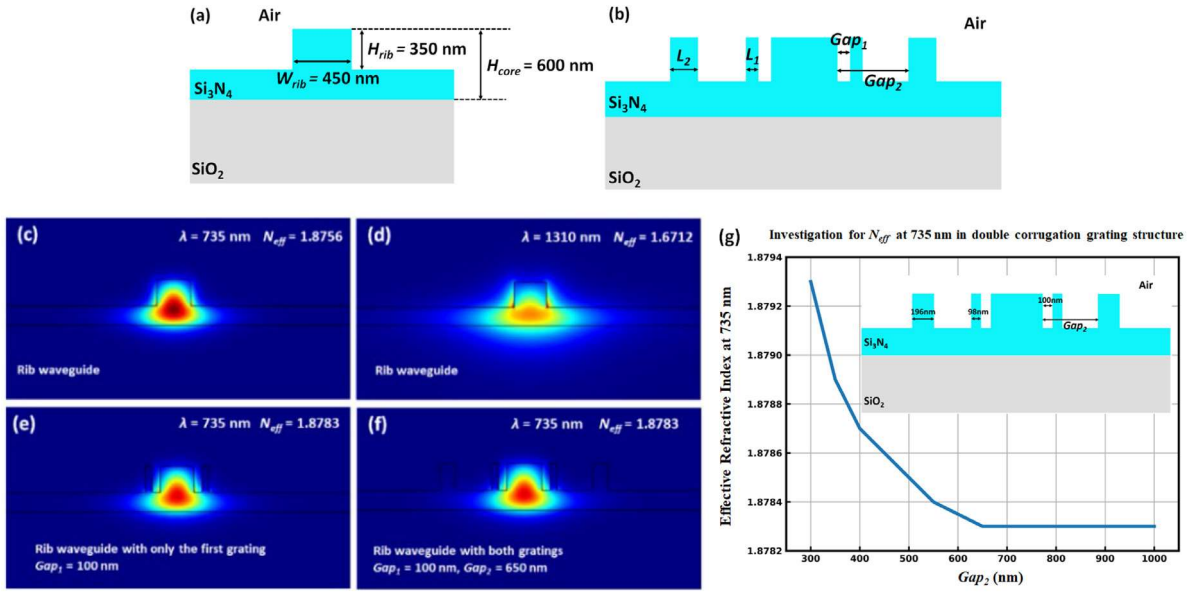

Fig. 2. (a) Cross-section of the rib waveguide with labeled dimensions. (b) Cross-section of the rib waveguide with double corrugation gratings. (c) Mode profile at λ_1 in the rib structure. (d) Mode profile at λ_2 in the rib structure. (e) Mode profile at λ_1 in a single grating rib waveguide ($Gap_1 = 100$ nm). (f) Mode profile at λ_1 in the rib waveguide with the two gratings ($Gap_1 = 100$ nm, $Gap_2 = 650$ nm). (g) The mode effective index at λ_1 versus Gap_2 when $Gap_1 = 100$ nm. (TE-like polarization in all cases).

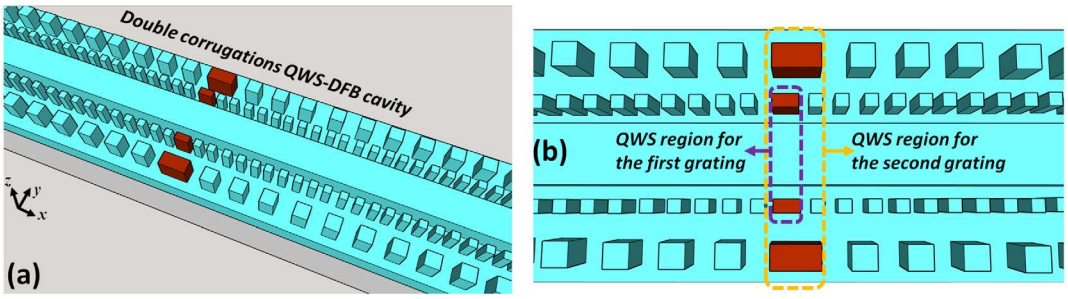

Fig. 3. (a) 3D schematic diagram of the proposed double corrugation QWS-DFB cavity structure, the deep red parts representing shifted regions. (b) Top view for the center of the double corrugation QWS-DFB cavity, the shifted regions of the first gratings and the second gratings are labeled, respectively.

Table 1
Parameters for the double corrugation QWS-DFB.

Bragg grating label	First grating	Second grating
Target wavelength	$\lambda_1 = 735$ nm	$\lambda_2 = 1310$ nm
Effective refractive index	$N_{eff1} = 1.8756$	$N_{eff2} = 1.6712$
Bragg period	$\Lambda_1 = 196$ nm	$\Lambda_2 = 392$ nm
Filling factor	$f_1 = 0.5$	$f_2 = 0.5$
Single square grating length and width	$L_1 = 98$ nm	$L_2 = 196$ nm
Grating period number	$N_1 = 2000$	$N_2 = 1000$
Distance Between rib waveguide and gratings	$Gap_1 = 100$ nm	$Gap_2 = 650$ nm
Coupling coefficient	$\kappa_1 = \sim 7400\ m^{-1}$	$\kappa_2 = \sim 3200\ m^{-1}$
Mode area	$A_1 = 0.3668\ \mu m^2$	$A_2 = 0.9136\ \mu m^2$
Mode overlap [25]	0.818	

field distributions along the cavity were analyzed. For a better comparison, we performed identical 3D-FDTD simulations for the two sets of structures comprising only one of the two gratings. Fig. 4(a) and (b) show the transmission results near λ_1 and λ_2, respectively, meanwhile the resonance around λ_1 is shown in a zoom in view in Fig. 4(a) in order to have a clear look on it due to its higher Q factor. The electrical field distribution of these two resonances in the double corrugation cavity are plotted in Fig. 4(c) and (d), respectively.

As visible, two resonances with ~590 nm frequency separation were obtained, confirming and validating the whole design approach. The green dotted line in Fig. 4(a) and the black dashed line in Fig. 4(b) are both flat and close to 1, which successfully proves that: (i) Short wavelengths (around λ_1) cannot feel the presence of the outer gratings due to a laterally compressed mode profile; (ii) The inner gratings effectively act as a sub-wavelength structure for large wavelengths around λ_2, thus precluding diffractive effects and undesired losses. Additionally, in Fig. 4(a), the transmission results near λ_1 in the complete grating structure and when only the inner gratings are considered are the same, while around λ_2 a little red shift occurs when the simulated structure is changed from the structure containing only the outer gratings to the true double grating geometry. Physically, the optical mode at λ_1 is indeed too compressed laterally to feel the presence of the outer gratings, while at λ_2, the effective refractive index of the mode slightly increases when the first gratings are introduced, leading to a slight resonance red shift. Of course, this shift could be compensated by a predesign step according to application requirements. From the simulation

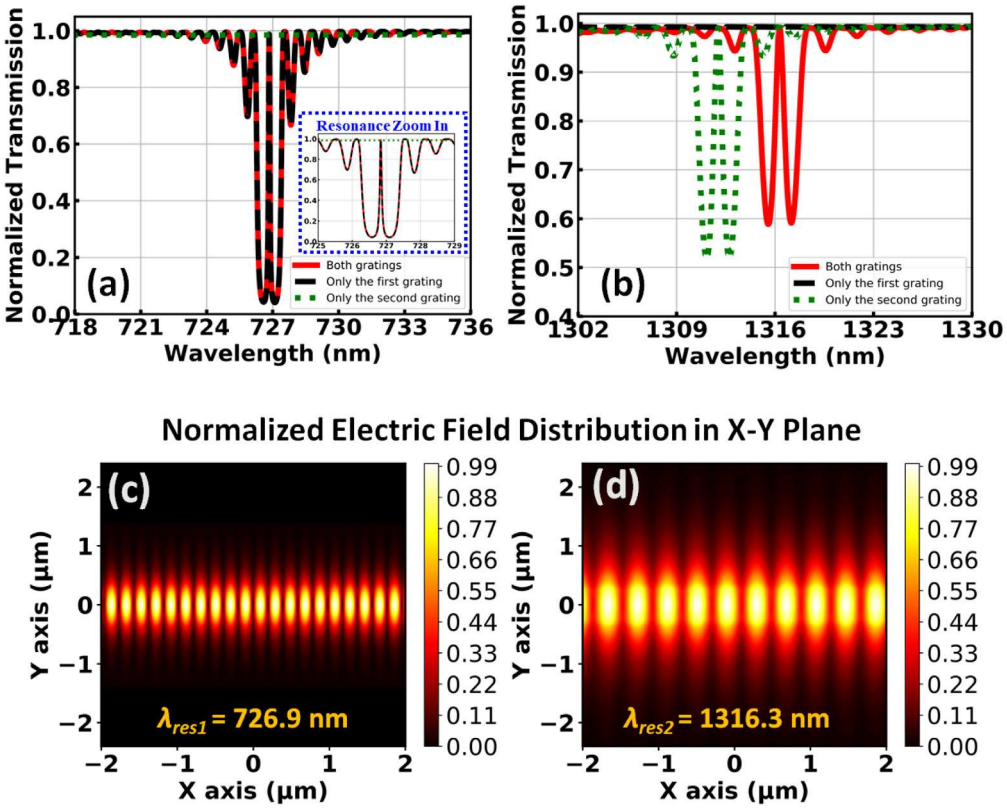

Fig. 4. 3D-FDTD simulation results. (a) Transmission results near λ_1 (short resonance wavelength). (b) Transmission results near λ_2 (long resonance wavelength). (c) Normalized electric field distribution at λ_{res1} = 726.9 nm in the double corrugation QWS-DFB cavity. (d) Normalized electric field distribution at λ_{res2} = 1316.3 nm in the double corrugation QWS-DFB cavity.

results, Q values at λ_1 and λ_2 were estimated as ~11000 (Q_1) and ~1500 (Q_2), respectively. In the example study case, regarding to the computing time consuming, a geometry with only 2000 periods for the inner gratings (so 1000 periods for the outer ones) was considered, leading to acceptable Q values but limited to ~10^4. However, benefiting from the flexibility of the design approach, such acceptable values for light–matter interaction reinforcement could be enlarged, for example by increasing the numbers of grating periods.

4. Conclusion

We propose a design strategy to achieve two resonances with huge wavelength separation being supported simultaneously in a double corrugation distributed feedback cavity (separated as 590 nm in the investigated typical example). The key idea in the proposed approach is to operate in conditions where the two sets of grating corrugations act nearly independently and to avoid diffraction effects simultaneously. At the shorter wavelengths, the waveguide mode profile is too compressed to feel the introduced outer gratings, thus only interfering with the inner gratings. For the longer wavelengths, on the contrary, the inner gratings are designed to operate as a sub-wavelength pattern. In the investigated studied example case, simulated by 3D-FDTD method, resonances at ~727 nm and ~1316 nm were produced in a designed double corrugation waveguide cavity, exhibiting ~11000 and ~1500 quality factors, respectively. We think that this double distributed feedback approach provides a path for effectively designing doubly resonant structures with two controllable far-separated resonances in single waveguide cavity structures. Applications to nonlinear optical process, sensing, lasing and amplification in on-chip photonic platforms could take benefit of this simple and flexible proposed method.

Declaration of competing interest

The authors declare that they have no known competing financial interests or personal relationships that could have appeared to influence the work reported in this paper.

Acknowledgments

We thank the OpticAll ANR French national project as well as the China Scholarship Council for supporting this work.

References

[1] A. Ramachandran, et al., A universal biosensing platform based on optical micro-ring resonators, Biosens. Bioelectron. 23 (7) (2018) 939–944.
[2] Z. Tu, D. Gao, M. Zhang, D. Zhang, High-sensitivity complex refractive index sensing based on Fano resonance in the subwavelength grating waveguide micro-ring resonator, Opt. Express 25 (17) (2017) 20911–20922.
[3] L. Jin, M. Li, J.J. He, Highly-sensitive silicon-on-insulator sensor based on two cascaded micro-ring resonators with vernier effect, Opt. Commun. 284 (1) (2011) 156–159.
[4] O. Jafari, W. Shi, S. Larochelle, Mach–Zehnder silicon photonic modulator assisted by phase-shifted Bragg gratings, IEEE Photon. Technol. Lett. 32 (8) (2020) 445–448.
[5] E.O. Potma, C. Evans, X.S. Xie, R.J. Jones, J. Ye, Picosecond-pulse amplification with an external passive optical cavity, Opt. Lett. 28 (19) (2003) 1835–1837.
[6] M. Pollnau, J.D.B. Bradley, Optically pumped rare-earth-doped Al2O3 distributed-feedback lasers on silicon [Invited], Opt. Express 26 (18) (2018) 24164–24189.
[7] H. Rong, et al., A continuous-wave Raman silicon laser, Nature 433 (2005) 725–728.
[8] X. Lu, S. Rogers, W.C. Jiang, Q. Lin, Selective engineering of cavity resonance for frequency matching in optical parametric processes, Appl. Phys. Lett. 105 (2014) 151104.
[9] M. Soljacic, J.D. Joannopoulos, Enhancement of nonlinear effects using photonic crystals, Nat. Mater. 3 (2004) 211–219.

[10] M.H.P. Pfeiffer, et al., Octave-spanning dissipative Kerr soliton frequency combs in Si3N4 microresonators, Optica 4 (7) (2017) 684–691.
[11] M.H. Anderson, et al., Photonic chip-based resonant supercontinuum, Aug. 2019, arXiv preprint arXiv:1909.00022 [physics.optics].
[12] W. Bogaerts, et al., Silicon microring resonators, Laser Photonics Rev. 6 (1) (2012) 47–73.
[13] B. Song, S. Noda, T. Asano, Y. Akahane, Ultra-high-Q photonic double-heterostructure nanocavity, Nat. Mater. 4 (2005) 207–210.
[14] E. Kuramochi, H. Taniyama, T. Tanabe, K. Kawasaki, Y. Roh, M. Notomi, Ultrahigh-Q one-dimensional photonic crystal nanocavities with modulated mode-gap barriers on SiO2 claddings and on air claddings, Opt. Express 18 (15) (2010) 15859–15869.
[15] P.B. Deotare, M.W. McCutcheon, I.W. Frank, M. Khan, M. Lončar, High quality factor photonic crystal nanobeam cavities, Appl. Phys. Lett. 94 (2009) 121106.
[16] J.S. Foresi, et al., Photonic-bandgap microcavities in optical waveguides, Nature 390 (1997) 143–145.
[17] Y. Zhang, M.W. McCutcheon, I.B. Burgess, M. Loncar, Ultra-high-Q TE/TM dual-polarized photonic crystal nanocavities, Opt. Lett. 34 (17) (2009) 2694–2696.
[18] K. Rivoirea, S. Buckley, J. Vučković, Multiply resonant high quality photonic crystal nanocavities, Appl. Phys. Lett. 99 (2011) 013114.
[19] K. Rivoirea, S. Buckley, J. Vučković, Multiply resonant photonic crystal nanocavities for nonlinear frequency conversion, Opt. Express 19 (22) (2011) 22198–22207.
[20] G. Singh, et al., Resonant pumped erbium-doped waveguide lasers using distributed bragg reflector cavities, Opt. Lett. 41 (6) (2016) 1189–1192.
[21] E. Durán-Valdeiglesias, et al., Tailoring carbon nanotubes optical properties through chirality-wise silicon ring resonators, Sci. Rep. 8 (2018) 11252.
[22] P.J. Bock, et al., Subwavelength grating periodic structures in silicon-on-insulator: a new type of microphotonic waveguide, Opt. Express 18 (19) (2010) 20251–20262.
[23] Robert Halir, et al., Robert halir others waveguide sub-wavelength structures: a review of principles and applications, Laser Photonics Rev. 9 (1) (2015) 25–49.
[24] https://www.comsol.
[25] https://support.lumerical.com/hc/en-us/articles/360034396834-Understanding-the-mode-overlap-calculation.
[26] W.H. Bragg, W.L. Bragg, The reflection of X-rays by crystals, Proc. R. Soc. Lond. Ser. A. Math. Phys. Eng. Sci. 88 (605) (1913) 428–438.
[27] T.E. Murphy, Design, Fabrication and Measurement of Integrated Bragg Grating Optical Filters (Ph.D. dissertation), Cambridge, MA, USA, 2001.
[28] X. Wang, Silicon Photonic Waveguide Bragg Gratings (Ph.D. dissertation), Univ. of British Columbia, Vancouver, Canada, 2013.
[29] Z. Tu, J. Zhang, J. Rönn, C. Alonso-Ramos, X. Leroux, L. Vivien, Z. Sun, E. Cassan, Potential for sub-mm long erbium-doped composite silicon waveguide DFB lasers, Sci. Rep. 10 (2020) 10878.
[30] https://www.lumerical.com.